

Mechanical fault interaction within the Los Angeles Basin: A two-dimensional analysis using mechanical efficiency

Michele L. Cooke

Geosciences Department, University of Massachusetts-Amherst, Amherst, Massachusetts, USA

Ayako Kameda¹

Geology and Geophysics Department, University of Wisconsin-Madison, Madison, Wisconsin, USA

Received 23 March 2001; revised 13 December 2001; accepted 18 December 2001; published 26 July 2002.

[1] Mechanical models examine deformation within eight different structural cross sections proposed by *Davis et al.* [1989] and *Shaw and Suppe* [1996] along a northeast-southwest transect across the Los Angeles Basin, California. Horizontal contraction of the models, constrained by geodetic measurements, yields varying dip-slip rates along frictionally sliding faults within the different cross sections. Mechanical efficiency analysis using effective stiffness and strain energy density assesses the overall fault system deformation as well as the partitioning of work between fault slip and host rock strain. The cross section interpreted by *Shaw and Suppe* [1996] has the best fit to paleoseismically determined slip rates and the greatest mechanical efficiency (greatest proportion of work toward fault slip); however, this model produces excessive reverse slip along the Newport-Inglewood fault. A modified fault configuration with a wedge or blind Puente Hills thrust fault rather than a ramp-detachment configuration better matches the paleoseismic data with slightly lower mechanical efficiency. Slip rates in the mechanical models based on interpretations of *Shaw and Suppe* [1996] have much closer match to the geologically determined rates than those estimated from kinematic models. This difference is due to (1) differing time spans of slip rate estimates and (2) deformable rather than rigid host rock in the mechanical models. The mechanical efficiency analysis provides quantitative indicators of overall fault system deformation, including the cumulative effect of interaction between individual faults. Assessment of effective stiffness and strain energy density furthers our understanding of two-dimensional fault interactions in the Los Angeles Basin and offers great potential for future applications. *INDEX TERMS:* 8015

Structural Geology: Local crustal structure; 8010 Structural Geology: Fractures and faults; 8020 Structural Geology: Mechanics; 8005 Structural Geology: Folds and folding; *KEYWORDS:* fault interaction, mechanical models, active faulting, Los Angeles

1. Introduction

[2] The Los Angeles Basin lies at the juncture between the Peninsular Ranges and the Transverse Ranges of southern California. Active crustal deformation of this region is expressed as slip along a three-dimensional system of interacting faults [e.g., *Yerkes*, 1965; *Davis et al.*, 1989; *Wright*, 1991; *Shaw and Suppe*, 1996; *Shen et al.*, 1996; *Walls et al.*, 1998]. Active NW trending faults include the Whittier-Elsinore, Newport-Inglewood, and Palos Verdes faults, whereas active E-W trending fault systems include the Malibu-Santa Monica-Raymond Hill fault system at the northern edge of the basin [*Yerkes*, 1965; *Wright*, 1991; *Shen et al.*, 1996] (Figure 1). These faults are believed to interact via a subsurface system of horizontal detachments

and thrust ramps at about 10–15 km depth [*Davis et al.*, 1989; *Shaw and Suppe*, 1996]. Several active fault zones in the Los Angeles region have produced damaging historic earthquakes: 1933 Long Beach (*M* 6.3), 1971 San Fernando (*M* 6.7), 1987 Whittier Narrows (*M* 6.0), and 1994 Northridge (*M* 6.7) [*Hauksson and Jones*, 1989; *Jones et al.*, 1994]. In particular, earthquakes on unexposed and therefore underrecognized blind thrust faults such as the 1987 Whittier Narrows (*M* 6.0) and 1994 Northridge (*M* 6.7) have caused more than \$25 billion dollars in damage [*Davis et al.*, 1989; *Hauksson and Jones*, 1989; *Jones et al.*, 1994]. Recognizing these faults and characterizing their configuration and slip rates are critical steps toward developing accurate earthquake source characteristics, such as likely area of fault rupture, for predictive earthquake algorithms used to calculate seismic hazard in the Los Angeles Basin [e.g., *Schenk*, 1989; *Petersen et al.*, 1996].

[3] This study examines the mechanical interaction among faults within several previously proposed NE-SW structural sections across the Los Angeles Basin. Because

¹Now at Geological and Environmental Sciences Department, Stanford University, Stanford, California, USA.

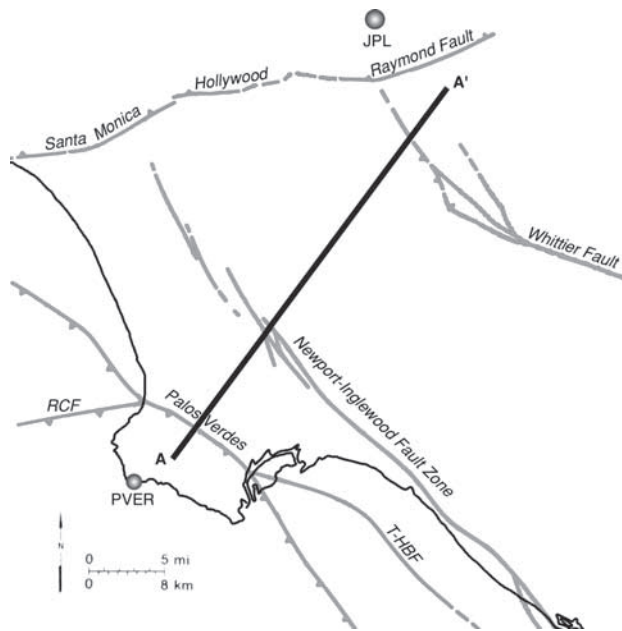


Figure 1. Fault map of the Los Angeles Basin, California (based on *Wright* [1991]). The bold line marks the approximate trace of the investigated cross sections. The position and bearing of the transects across the Los Angeles Basin vary slightly. The circles indicate positions of the GPS stations (PVER and JPL) used to determine regional strain [*Feigl et al.*, 1993]. RCF, Redondo Canyon Fault; T-HBF, THUMS-Huntington Beach fault.

multiple fault configurations that match observations have been proposed using kinematic reconstruction methods [*Davis et al.*, 1989; *Wright*, 1991; *Shaw and Suppe*, 1996], a mechanical comparison of these models may yield insight into the most viable subsurface fault configuration for the Los Angeles Basin. The most viable mechanical model of interacting faults will have slip rates that match the available paleoseismic rates under horizontal contraction constrained by recent geodetic measurements. The faults within the model are prescribed frictional rheology so that tractions and slip on the faults need not be known a priori. Additionally, this study explores the mechanical efficiency of the proposed fault systems to explore the partitioning of strain into fault slip and host rock deformation. Mechanical efficiency provides a means to quantify the overall behavior of an interacting system of faults and provides insight into deformation throughout the system.

1.1. Geologic and Paleoseismic Setting

[4] In this paper we investigate faulting within the Los Angeles sedimentary basin from the Palos Verdes Peninsula and Pacific shoreline to the base of the San Gabriel Mountains. The central basin consists of Miocene, Pliocene, and Pleistocene sedimentary strata more than 5 km thick [e.g., *Norris and Webb*, 1990]. The underlying basement rock of the central and northeastern basin is slightly metamorphosed sedimentary Jurassic rocks that have been intruded by late Cretaceous granites [*Norris and Webb*, 1990]. In contrast, the basement of the southwestern part of the Los Angeles Basin (from the Newport-Inglewood

fault zone to the Palos Verdes Peninsula and western shore) consists of Catalina schist of the Franciscan Formation.

[5] Extension and subsequent formation of the Los Angeles Basin initiated during the Miocene and continued through the Pliocene [*Wright*, 1991; *Nicholson et al.*, 1994; *Shen et al.*, 1996]. The transition to present-day transpressional tectonics began at ~ 4 Ma and was associated with a change in relative plate motion between the Pacific and North American plates; this transpression has produced the present northwest-southeast trending basin geometry [e.g., *Wright*, 1991; *Yeats and Beall*, 1991; *Ingersoll and Rumelhart*, 1999]. Some currently active faults in the Los Angeles region are believed to have originally formed in the extensional tectonic setting of Miocene-Pliocene and later were reactivated in the changing tectonic regime [e.g., *Wright*, 1991; *Shaw and Suppe*, 1996].

[6] Recent fault slip rates within the basin have been constrained from limited direct and indirect paleoseismic evidence [e.g., *Clark et al.*, 1984; *Petersen and Wesnousky*, 1994]. Two faults within the basin with sufficient surface data to estimate slip rates are the Palos Verdes and Newport-Inglewood faults. Deformation along the Palos Verdes fault is expressed as both fault slip and uplift of the associated anticline, resulting in uplifted marine terraces [*Bryant*, 1987; *Fischer et al.*, 1987; *Ward and Valensise*, 1994; *McNeilan et al.*, 1996]. Reverse dip-slip rates of 0.38 mm/yr have been determined along the Palos Verdes fault from geologic evidence detected via shallow geophysical methods [*McNeilan et al.*, 1996]. The strike-slip rate along Palos Verdes fault has been evaluated from onshore seismic reflection data and geomorphology as 2.5–3.8 mm/yr [*Stephenson et al.*, 1995]. The long-term strike-slip rate along the Newport-Inglewood fault, constrained by geologic offsets, is ~ 0.5 mm/yr [*Freeman et al.*, 1992]; however, paleoseismic evidence suggests a wide range of Holocene slip rates for the fault depending on the location along strike [*Grant et al.*, 1997]. The estimated right-lateral slip rates range from 0.03–0.05 mm/yr in Signal Hill in Long Beach [*Suppe et al.*, 1992] to 0.34–0.55 mm/yr in coastal Orange County [*Grant et al.*, 1997]. Representative dip-slip rates associated with the Newport-Inglewood fault are elusive because right-lateral strike slip along the echelon faults comprising the Newport-Inglewood fault produces a series of local uplifts and grabens [*Harding*, 1973; *Grant et al.*, 1997]. Measurements of vertical separation rate, such as at Baldwin Hills [*Clark et al.*, 1984] or Coastal Orange County [*Grant et al.*, 1997], have been taken along one side of grabens and uplifts between faults steps and are non-representative of dip slip of the fault zone [*Grant et al.*, 1997]. Although considerable uplift has been measured along the Newport-Inglewood fault zone (e.g., 5–8 mm/yr at Baldwin Hills [*Bandy and Marincovich*, 1973] and 0.18 m coseismic uplift associated with the 1933 Long Beach earthquake [*Castle and Buchanan-Banks*, 1989]), this uplift may result from local folding associated with wrench faulting rather than significant quaternary dip slip along the Newport-Inglewood fault [*Harding*, 1973; *Yeats*, 1973; *Wright*, 1991]. Cross sections and structure contour maps developed from subsurface data show that the net vertical separation of strata across each of the folds is nearly zero, and this separation does not have consistent sense (e.g., east

side up) among the folds [Harding, 1973; Wright, 1991]. Furthermore, seismicity along the Newport-Inglewood trend suggests predominately right-lateral faulting with secondary reverse slip and normal faulting [Hauksson, 1987].

[7] Aside from the Palos Verdes and Newport-Inglewood faults, most faults of the Los Angeles Basin, including two that produced the recent Whittier Narrows and Northridge earthquakes, are buried and therefore inaccessible to paleoseismic investigations. The lack of direct observation of these faults compels us to make better use of indirect data and deterministic fault models in order to infer slip rates.

[8] Ongoing monitoring of permanent Global Positioning System (GPS) stations in southern California has allowed the calculation of current surface deformation rates in the Los Angeles region. The relative velocity between the Palos Verdes and Jet Propulsion Laboratory (Pasadena) GPS stations (Figure 1) suggests $5.0 \pm 1.2 \text{ mm yr}^{-1}$ of NE-SW (San Andreas perpendicular) contraction and $0.2 \pm 1.2 \text{ mm yr}^{-1}$ of right-lateral shear parallel to the San Andreas fault trend [Feigl *et al.*, 1993]. This NE-SW shortening rate is equivalent to an overall strain rate of $\sim 9.0 \cdot 10^{-8} \text{ yr}^{-1}$. Paleoseismic evidence suggests that the current geodetic contraction rate has been consistent through the last million years; for example, the Palos Verdes fault displays relatively uniform uplift of younger than 1 Ma marine terraces [Ward and Valensise, 1994].

1.2. Kinematic Interpretations of Subsurface Fault System

[9] Geologic cross sections have been interpreted along a SW-NE transect across the Los Angeles Basin from Palos Verdes Hills to the Whittier/Repetto Hills [Davis *et al.*, 1989; Wright, 1991; Shaw and Suppe, 1996]. These cross sections have been developed using several different methods: (1) retrodeformable cross-section method [Davis *et al.*, 1989], (2) fault-related fold theories and growth strata analysis along with newly available seismic and borehole data [Shaw and Suppe, 1996], and (3) integration with regional geology [Wright, 1991]. The cross sections developed by these three groups, using the different methods, exhibit very different styles of faulting (Figure 2). The NE-SW cross section of the Los Angeles Basin interpreted by Wright [1991] has isolated linear and curved high-angle (steep) faults near the surface (Figure 2). Wright [1991] refrains from interpreting deeper levels of faulting where data are scarce. Davis *et al.* [1989] interpret seven possible cross-sections that match the available observations. Two representative cross sections shown in Figure 2 contain isolated and steep faults within the upper few kilometers of the section as well as a deep connected system of low-angle ramps and horizontal detachments with occasional duplexes (see Appendix A for other fault configurations proposed by Davis *et al.* [1989]). Shaw and Suppe [1996] also present several slight variations of their interpreted fault system but showcase the interpretation shown in Figure 2, which contains a connected system of steep faults, ramps, and horizontal detachments.

[10] Using the kinematic relationships between fault slip, fold shape, and the deposition of new strata, fault slip amount can be estimated within the interpreted cross sections. Furthermore, by constraining the onset of fold growth (e.g., from stratigraphic evidence), slip rates have been

inferred on the interpreted faults [Davis *et al.*, 1989; Shaw and Suppe, 1996]. Owing to the location and the two-dimensional nature of the cross sections, comparison of the kinematically derived and available paleoseismic slip rates is limited to dip-slip rates for the Palos Verdes fault (Figure 3). Although the Shaw and Suppe [1996] slip rates are closer to the paleoseismic observations than those of the Davis *et al.* [1989] models, all of the kinematically derived dip-slip rates are several times larger than the paleoseismic observations. Explanations for this discrepancy include incorrect interpretation of fault geometry and assumption of rigid host rock surrounding the fault surfaces [Shaw and Suppe, 1996]. The kinematic models assume that all deformation occurs as slip along the fault surfaces, leaving the host rock relatively undeformed.

[11] This study employs mechanical numerical boundary element method (BEM) experiments on the eight proposed cross sections in order to evaluate the mechanical viability of the various cross-sections. The proposed section by Wright [1991] is not included in the side-by-side comparison of models because deep levels of faulting are not inferred in this cross section. Consequently, this study compares the eight cross sections developed using kinematic balancing methods. The mechanical models of this study employ remote boundary conditions based on current geodetic strain rates measured across the basin and frictionally sliding faults. In contrast with the kinematic models, the BEM models incorporate elastic deformation of the host rock around fault surfaces so that the resulting slip rates may differ from kinematic estimates. The most viable mechanical model of Los Angeles faulting should have slip rates that match the available paleoseismic data. Furthermore, a mechanical efficiency analysis on each of the modeled cross sections highlights the work of fault slip and the work of elastic strain of the host rock. This innovative analysis allows us to investigate the overall behavior of the fault system and the influence of various fault interactions on the entire fault system.

2. Boundary Element Method

[12] Studies of multiple fault interactions can best be accomplished using numerical methods that solve the governing differential equations of continuum mechanics [e.g., Crouch and Starfield, 1990]. Numerical methods such as finite element method (FEM) and boundary element method (BEM) can simulate deformation associated with complex fault configurations and calculate stress and strain throughout the body from prescribed tractions or displacements on the model boundaries [e.g., Crouch and Starfield, 1990]. Unlike FEM, which requires discretization of the entire body, BEM only requires discretization of model boundaries and discontinuities (i.e., faults). This is advantageous for modeling multiple interacting faults because BEM requires less effort for discretization, and errors due to discretization and approximations arise only on the boundaries and along fault surfaces [Crouch and Starfield, 1990].

[13] Our investigation of fault interaction employs a two-dimensional BEM code (FRIC2D) which computes elastic and inelastic deformation associated with frictional slip along faults [Cooke and Pollard, 1997]. FRIC2D uses the

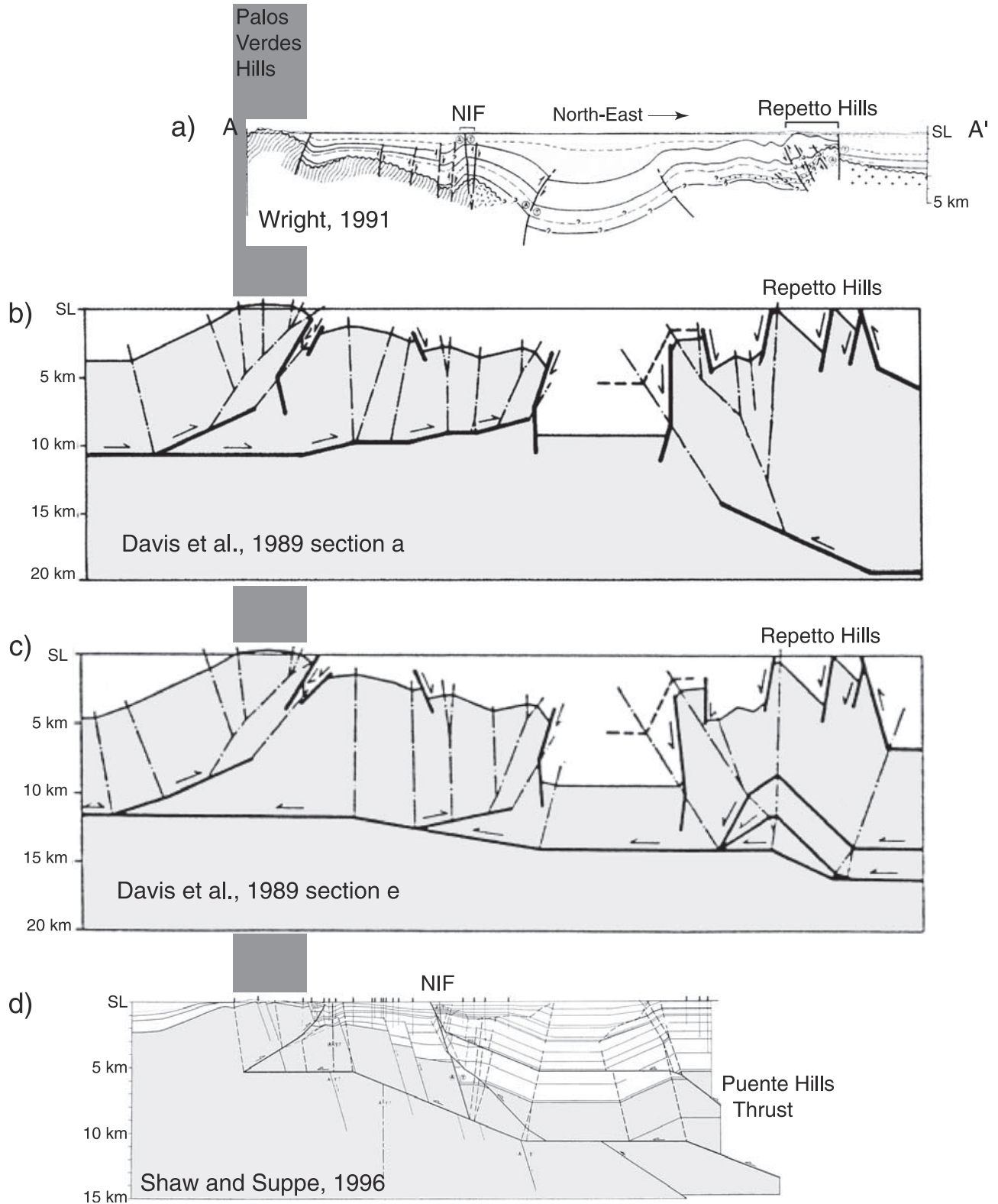


Figure 2. Four published NE-SW cross sections across the Los Angeles Basin. (a) Section based on correlation with regional geology (modified from *Wright* [1991]) (NIF, Newport Inglewood fault). (b and c) Cross sections developed from kinematic reconstructive methods (modified from *Davis et al.* [1989]). (d) Cross section developed from fault-related folding kinematics as well as recently released seismic and well data (modified from *Shaw and Suppe* [1996]). The four cross sections across the Los Angeles Basin have identical scale and are aligned to the position of Palos Verdes Hills.

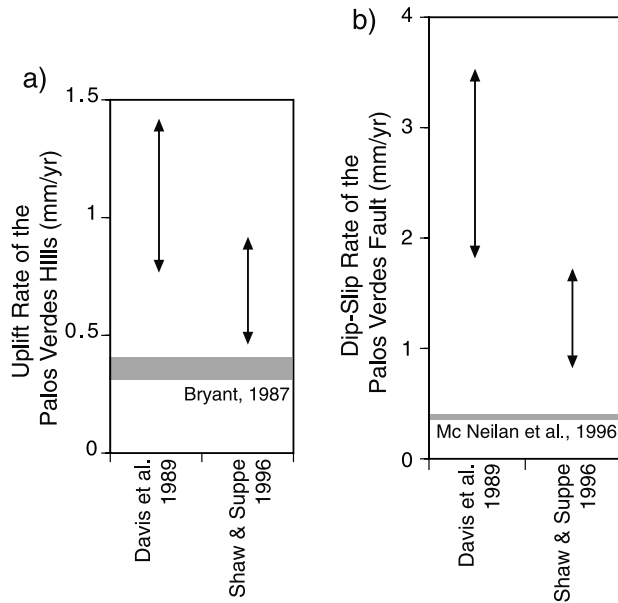


Figure 3. Comparison of paleoseismic and kinematically derived dip-slip rates for the Palos Verdes fault. Horizontal bar shows paleoseismic rate; bar thickness indicates data range. Paleoseismic dip-slip rate is based on offsets of Holocene channels revealed by shallow geophysics [McNeilan et al., 1996].

displacement discontinuity formulation of *Crouch and Starfield* [1990] with special constitutive frictional-slip elements. The model boundaries and faults are discretized into linear elements of equal length each with shear and normal displacement discontinuities, both of which remain constant along the length of each element. While the elements along the model boundaries require prescription of either tractions or displacements, the fault elements require only prescription of the faults' constitutive properties (i.e., frictional strength). Within FRIC2D, fault elements accommodate inelastic frictional slip through the following constitutive parameters: shear stiffness, normal stiffness, cohesion, and coefficient of friction [Crouch, 1979; Cooke and Pollard, 1997]. The incorporation of constitutive frictional elements allows for more realistic fault interaction than boundary elements that require prescription of tractions or slip along fault elements. Rather than prescribing the fault deformation, within FRIC2D faults slip in response to fault rheology, lithostatic compression, and fault interaction. FRIC2D has been used to investigate the early stages of fault-related fold development [Cooke and Pollard, 1997], bedding plane slip within folds [Cooke et al., 2000], joint propagation near bedding planes [Cooke and Underwood, 2001], and blind thrust fault propagation [Roering et al., 1997].

[14] This study utilizes these constitutive frictional-slip elements to simulate fault slip within the Los Angeles Basin while applying NE-SW contraction prescribed as displacement along the model boundaries. Our mechanical models simplify the complex geology of the region in two ways: two-dimensional deformation style and uniform material composition. Although the Los Angeles region is deforming via a complex three-dimensional system of active faults, the

two-dimensional assessment of this and previous studies provides understandings of fault interactions that can serve as guidelines for three-dimensional fault interaction. Another limit of the numerical BEM models is that they assume uniform material properties of the host rock. Incorporating the heterogeneity of sedimentary strata overlying granitic and metamorphic basement rocks may more accurately simulate deformation within this region than our simplified homogeneous model but would also require more sophisticated modeling tools than those currently available to us. By assuming homogeneous material properties, we focus on the first-order effects of fault geometry on fault interaction, mechanical efficiency and slip rate.

3. Mechanical Efficiency

[15] The mechanical energy budgets of deforming fold-and-thrust belts have been analyzed by analogy to wedges of soil or snow that deform in front of a moving bulldozer; these analyses utilize the premise that the fault system or deforming wedge grows by minimizing the work done [e.g., Mitra and Boyer, 1986; Dahlen and Barr, 1989]. Similarly, fault systems may evolve to increase their overall mechanical efficiency so that an efficient fault system is analogous to a bulldozer consuming little energy (gasoline) to deform snow. Several observations of fault system evolution support our proposition that fault systems evolve toward greater efficiency. The number of echelon steps per unit length of active strike-slip faults has been observed to decrease with cumulative geological offset [Wesnousky, 1988]. Initially rough fault surfaces undergo abrasive wear and become smoother as faults slip [Scholz, 1990]. Similarly, stratigraphic evidence suggests that some extensional fault systems have evolved structurally to achieve a smoother and more efficient configuration [Gupta et al., 1998].

[16] The evolution of fault systems occurs with the accumulation of earthquakes and the development of new fault surfaces. In a system of multiple faults, local slip may cause stress adjustments [e.g., Cowie et al., 1995; An and Sammis, 1996; Kagan, 1997; Harris, 1998] that encourage fault system reorganization. The resulting fault configuration may have greater mechanical efficiency. For this study we assess the global (overall) mechanical efficiency of the proposed cross-sections of the Los Angeles Basin using two indicators: effective stiffness and average strain energy density.

[17] The first indicator of global mechanical efficiency, effective stiffness, measures the overall compliance of the fault system. Efficient fault systems are compliant (low effective stiffness) in that they produce large strains when loaded with relatively small stresses (i.e., the bulldozer uses little gasoline). The effective stiffness of the overall two-dimensional fault system, E' , undergoing contraction can be expressed as

$$E = \sigma_h / \epsilon_h, \quad (1)$$

where σ_h is the average horizontal normal stress that produces ϵ_h , the average horizontal contraction of the fault system. The fault system that requires the least stress to deform a given level of contraction has the lowest effective stiffness and is the most mechanically efficient. Effective

Table 1. Rock Material Properties Used in BEM Modeling^a

Property	Metamorphic (SW Basement) ~25%			Intrusive (NE Basement) ~25%		Sedimentary Cover ~50%			Average 100%
	Quartz-Sericite Schist	Quartz-Talc- Schist	Blue Schist	Biotite Quartz Diorite	Grano Diorite	Shale	Conglomerate	Sandstone	
Poisson's ratio	0.181 ^b	N/A	N/A	0.24 ^c	0.3 ^c	0.14 ^c	N/A	0.14 ^c	0.180
Young's modulus	60.0 ^c	N/A	N/A	68.6 ^c	70.2 ^c	51.5 ^c	77.9 ^c	55.5 ^c	63
Rock density, kg m ⁻³	2700 ^{c, b}	N/A	N/A	2740 ^c	2700 ^c	2770 ^c	2670 ^c	2650 ^c	2700

^aAverage material are calculated from estimated amounts of the different subsurface materials. Cross sections along the SW-NE transect across the Los Angeles basin contain approximately equal amounts of sedimentary and basement rocks. The basement rocks are composed of roughly equal amounts of metamorphic rocks in the southwest and intrusive rocks in the northeast. N/A indicates not available.

^bOwing to the scarcity of test data, the properties of Catalina schist were approximated from reported properties of quartz-sericite schist. The Poisson's ratio of quartz-sericite schist was taken from quartz-muscovite schist of *Birch* [1966].

^cValues are averaged from *Carmichael* [1984].

stiffness provides a convenient and intuitive measure of the compliance of an interacting system of faults. For comparisons of fault models with identical horizontal strain, such as in this study, the effective stiffness directly correlates with external work, which is one-half external stress times external strain.

[18] The second indicator of global mechanical efficiency used in this study is the average work done within the host rock or average strain energy density (SED). Strain energy density, V_0 , is the amount of work, in this case elastic strain energy, per unit volume [*Timoshenko and Goodier, 1934*]:

$$V_0 = \frac{1}{2} (\sigma_{xx}\epsilon_{xx} + \sigma_{yy}\epsilon_{yy} + \sigma_{zz}\epsilon_{zz} + 2\sigma_{xy}\epsilon_{xy} + 2\sigma_{xz}\epsilon_{xz} + 2\sigma_{yz}\epsilon_{yz}). \quad (2)$$

The plane strain conditions for the two-dimensional fault system requires that $\epsilon_{zz} = \epsilon_{yz} = \epsilon_{xz} = 0$ which reduces equation (2) to only three terms. To further simplify the strain energy density expression, we can apply the elastic constitutive equations (i.e., Hooke's law) to express the SED in terms of only stresses and elastic properties, E , Young's modulus and ν , Poisson's ratio [*Timoshenko and Goodier, 1934*]:

$$V_0 = \frac{(1 - \nu^2)}{2E} (\sigma_{xx}^2 + \sigma_{yy}^2) + \frac{(1 + \nu)}{E} (\sigma_{xy}^2 - \nu\sigma_{xx}\sigma_{yy}). \quad (3)$$

This work measures the amount of elastic strain energy stored at any point within the host rock. Rock adjacent to fault zones is far from undeformed and shows evidence of recent tectonic history [e.g., *Duebendorfer et al., 1998; Vermilye and Seeber, 1998*]. SED concentrations may arise in locally deformed regions, such as around fault tips. Correspondingly, SED shadows may develop adjacent to slipping faults where the elastic strain within the rock has been lessened. To quantify the overall SED of the entire fault system, we calculate the average SED throughout each of the models.

[19] Although the strain energy within the host rock calculates elastic strain, which is nonpermanent, the SED within the fault models could correlate with the level of inelastic strain of the host rock. For example, microcracking, creation of new fault surfaces, and other inelastic processes may occur within regions of high SED. Thus concentrations of SED, such as near fault tips, may serve as indicators of inelastic as well as elastic deformation of the host rock.

[20] These two indicators of mechanical efficiency quantify different aspects of work within the fault system. Effective stiffness represents the amount of external work done on the deforming system, so that efficient fault systems have lower effective stiffness than inefficient systems. In contrast, strain energy density examines work done within the host rock. High average SED indicates storage of strain within the host rock and inefficiency of the fault system, so that efficient fault systems have lower average SEDs.

[21] The purpose of the mechanical efficiency analysis in this study is to provide a quantitative method to assess the differences among the proposed cross sections for the Los Angeles Basin. The most viable fault model, shortened according to the geodetic data, will have fault slip rates that match the paleoseismic slip rates. This modeled section may or may not have the greatest mechanical efficiency. This technique provides an innovative and quantitative method for the comparison of deformation within fault systems. Our purpose here is to introduce this method

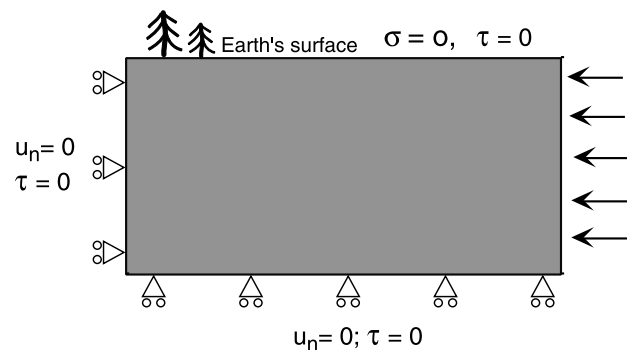


Figure 4. Boundary conditions for numerical models. The top of the model represents the traction-free surface of the Earth. The left and bottom of the model have zero shear traction and are allowed no normal displacement. The right side, representing the northeastern edge of the transect, is heaved to the left to simulate uniform horizontal contraction across the basin. The fault configurations of the models are based on cross sections proposed by *Davis et al. [1989]* and *Shaw and Suppe [1996]*. The models based on *Davis et al. [1989]* are 55 km long and 20 km deep, whereas the model of the *Shaw and Suppe [1996]* cross section is 44.5 km long and 15 km deep.

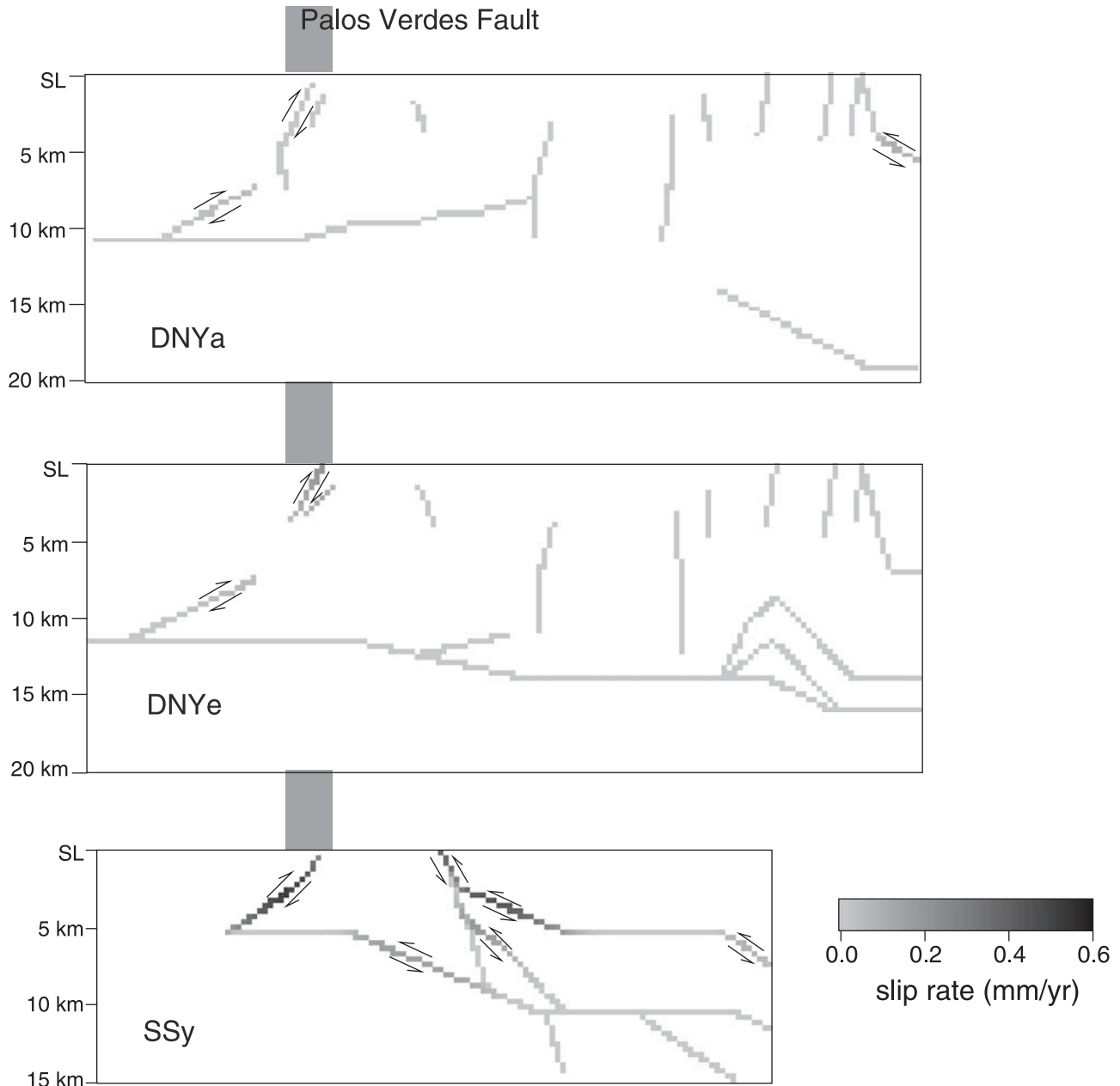


Figure 5. Slip distribution for three numerical models (results from other DNY models are presented in Appendix A). The faults that frictionally slip all show reverse slip sense, indicated by arrows. The maximum slip rate for DNYa, DNYe, and SSy is 0.09, 0.21, and 0.51 mm yr⁻¹, respectively.

and suggest ways in which it may facilitate future analysis of fault interaction.

4. Analysis of Proposed Cross Sections

4.1. Model Setup

[22] We prescribed the rock material properties in Table 1 to the host rock within the modeled fault systems proposed by *Davis et al.* [1989] and *Shaw and Suppe* [1996]. The elastic properties (e.g., Young's modulus and Poisson's ratio) used for this study are based on average properties of the rock types found in the Los Angeles region. The sedimentary units consist mostly of shale, conglomerate, and sandstone [*Reiter, 1984*]. The basement in the south-

western Los Angeles Basin consists of Mesozoic Catalina schist, which is categorized as quartz-sericite schist, quartz-talc-schist, and blue (glauconite) schist [*Reiter, 1984*]. The basement in the northeastern Los Angeles Basin consists of biotite quartz diorite and granodiorite [*Yerkes, 1965; Yeats and Beall, 1991*]. To examine the first-order effects of fault interaction within the Los Angeles Basin, we neglect material contrasts between these rock types and apply average properties within the model (Table 1). Lithostatic compression applied to the models corresponds to the average rock density of the region (Table 1).

[23] The modeled faults have uniform frictional resistance via prescription of a friction coefficient of 0.4. This friction coefficient is within the range of fault friction coefficients

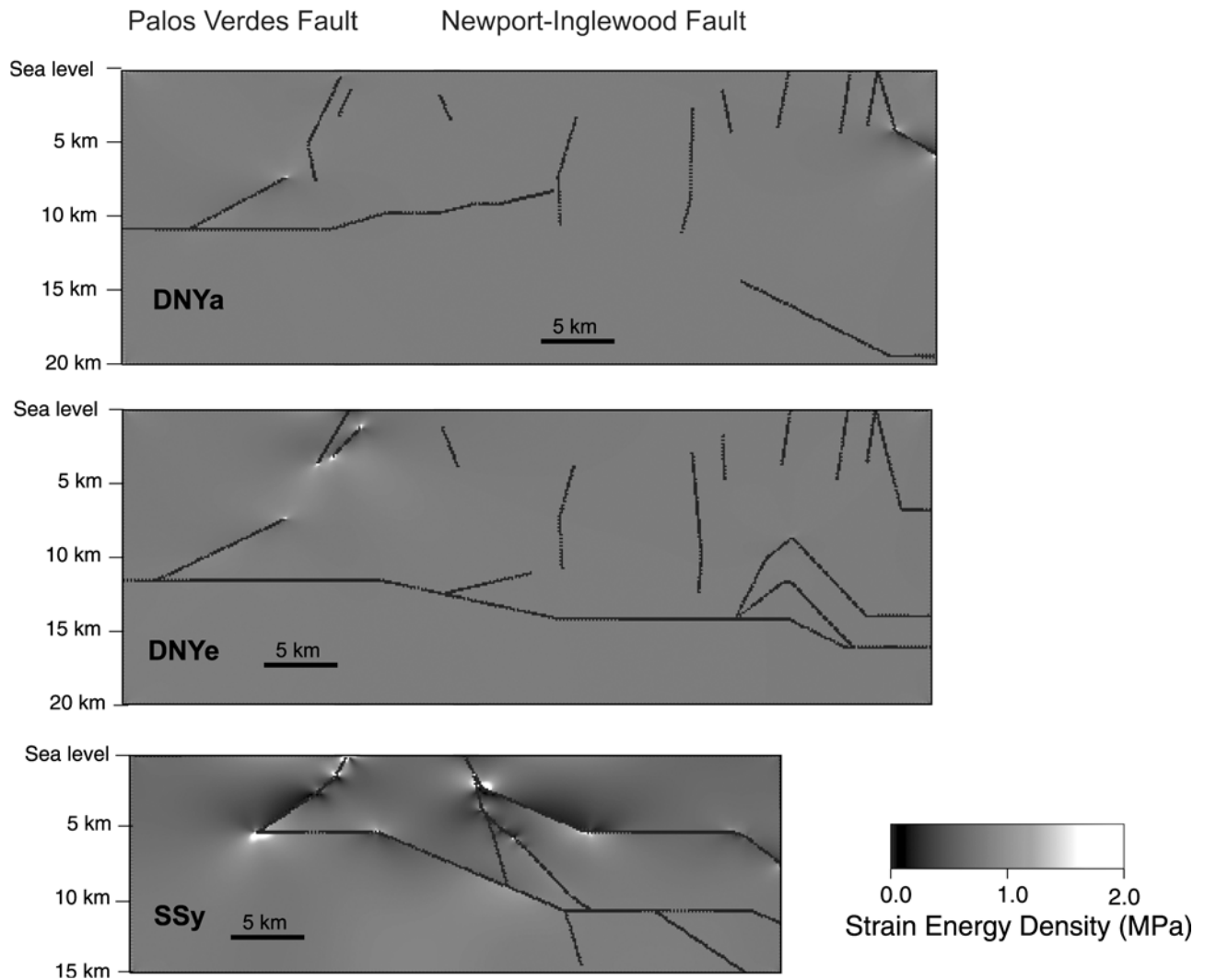


Figure 6. Strain energy density for three numerical models (results from the other DNY models are presented in Appendix A). Brighter colors indicate more intense stress concentrations. The *Shaw and Suppe* [1996] model has greater fault slip than the other models, which produces larger stress concentrations at fault bends. Correspondingly, this model also has the greatest strain shadows in the host material adjacent to the slipping faults.

suggested by previous researchers [e.g., *Scholz*, 1990; *Bird and Kong*, 1994; *King et al.*, 1994; *Deng and Sykes*, 1997; *Hardebeck et al.*, 1998; *Scholz*, 2000]. Regional models of southern California that vary friction coefficient to best match observed slip rates suggest lower friction coefficient along major faults [*Bird and Kong*, 1994]. However, *Bird and Kong* [1994] constrain all faults to have identical friction coefficient, and their study focuses on larger and more mature fault systems than those within the cross-sectional transect of this study. While the models of this study do not directly include pore pressure effects, net pore pressure effects are included in the value prescribed for the friction coefficient. The normal and shear fault stiffnesses of the fault surfaces are equivalent to those of the host rock.

[24] We prescribe uniform horizontal contractional strain of 0.5% by heaving the northeastern edge of the model toward the southwest (Figure 4). Using current strain rates [*Feigl et al.*, 1993], 0.5% contraction simulates 55,500 years

of deformation in the Los Angeles Basin. This time span greatly exceeds the estimated earthquake recurrence intervals along the faults [e.g., *Ward and Valensise*, 1994; *Dolan et al.*, 1995; *McNeilan et al.*, 1996; *Grant et al.*, 1997; *Dolan et al.*, 2000; *Oskin et al.*, 2000] so that most, if not all, of the faults within the Los Angeles Basin are expected to slip during the modeled time period. Thus, rather than modeling individual slip events, we investigate the cumulative deformation resulting from multiple earthquake events over many years using static frictional fault slip. Additionally, strain rate can be considered constant throughout the modeled time span because evidence from marine terraces younger than 1 Ma on Palos Verdes Hills display relatively uniform uplift [*Ward and Valensise*, 1994].

4.2. Mechanical Efficiency Results

[25] For ease of discussing the model results we employ a shorthand notation to refer to specific cross-sectional mod-

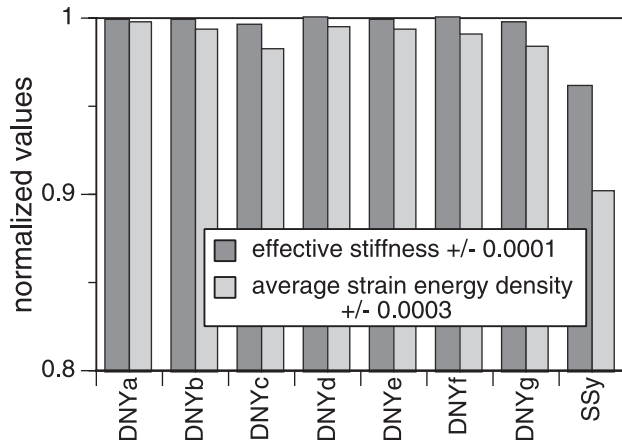


Figure 7. Normalized effective stiffness and average strain energy density of all eight mechanical models. The results are normalized to a faultless model. Errors were determined from the difference between models run to 100 and 99 iterations toward solution convergence. The SSy model has the lowest effective stiffness and the lowest average strain energy density; therefore SSy is the most mechanically efficient.

els. The models with fault configuration based on the seven *Davis et al.* [1989] cross sections are DNYa through DNYg. Similarly, the model with fault configuration based on cross-section Y-Y' of *Shaw and Suppe* [1996] is referred to as SSy.

[26] The amount of fault slip varies greatly among and within the cross sections (Figure 5). The SSy model has the greatest range of fault slip, from 0 mm yr⁻¹ along deep faults and horizontal detachments to 0.51 mm yr⁻¹ reverse slip along the Palos Verdes fault near the surface. Deep faults experience greater lithostatic detachment faults in these models are not suitably oriented for slip. Thus, shallow faults (depth <5 km) dipping ~30° are the most favorably located and oriented for frictional slip. The SSy model has much greater slip than any of the DNY models (Figures 5 and A1).

[27] Concentrations of SED occur near bends (kinks) of slipping faults within the models. In general, the SSy model produces more numerous and larger strain concentrations than the DNY models (Figure 6). Furthermore, the SSy model has pronounced strain shadows around slipping faults indicating that local elastic strain energy has been released by slip along the faults. The large concentration of SED within the SSy model can be attributed to the greater fault slip along favorably oriented gently dipping faults within this model. The largest strain concentrations occur at the intersections of interfering faults, such as the Palos Verdes ramp and the shallow detachment that meets this ramp at 5 km depth.

[28] The average SED, which represents the work of deforming the host rock, is lowest for the SSy model (0.9006 ± 0.0003; Figure 7). We normalize the average SED results to a model without faults in order to highlight the change in strain energy produced by the slipping fault system. Consequently, the strain energy due to lithostatic loading is not considered in the analysis. All cross sections modeled have lesser average SED than the faultless model (normalized values <1) because slip along the faults accom-

modates strain and releases elastic strain from the surrounding host rock. The errors for average SED and effective stiffness are determined from the discrepancies between models run for 99 and 100 iterations toward convergence. Absolute convergence was elusive for some models due to interference between adjacent slipping fault elements. The SSy model has by far the lowest average SED of all and is nearly 10% lower than the second lowest model (DNYc 0.9810 ± 0.0003).

[29] Effective stiffness, the measure of resistance to contraction, shows similar trends (Figure 7). SSy has the least normalized effective stiffness (0.9605 ± 0.0001), whereas the DNYa–g models have consistently high effective stiffness. The effective stiffness and average strain energy density results suggest that the cross section based on *Shaw and Suppe* [1996] has the greatest mechanical efficiency. Interestingly, we also observe highest SED concentrations at fault bends within the otherwise mechanically efficient SSy model (Figure 6). This suggests that locally inefficient fault interactions (e.g., fault bends) can be combined to produce an overall efficient fault system.

4.3. Slip Rates and Uplift Rates From Models

4.3.1. Palos Verdes fault

[30] Deformation along the Palos Verdes fault is expressed as both fault slip and uplift of the associated anticline, which uplifts former marine terraces [*Bryant, 1987; Fischer et al., 1987; Ward and Valensise, 1994; McNeilan et al., 1996*]. A reverse dip-slip rate of 0.38 mm yr⁻¹ has been determined along the Palos Verdes fault from geologic evidence detected via shallow geophysical methods [*McNeilan et al., 1996*].

[31] The Palos Verdes dip-slip rates from the mechanical models vary with fault configuration and range from <0.02 to 0.51 mm yr⁻¹ (Figure 8). The amount of reverse slip varies along the modeled faults because of increased lithostatic compression with depth and interaction with nearby faults. For this reason we calculate both the maximum slip, usually at the most shallow level of the fault, and average slip along sliding fault segments. The dip-slip rate along the Palos Verdes fault in SSy (0.38–0.51 mm yr⁻¹ average

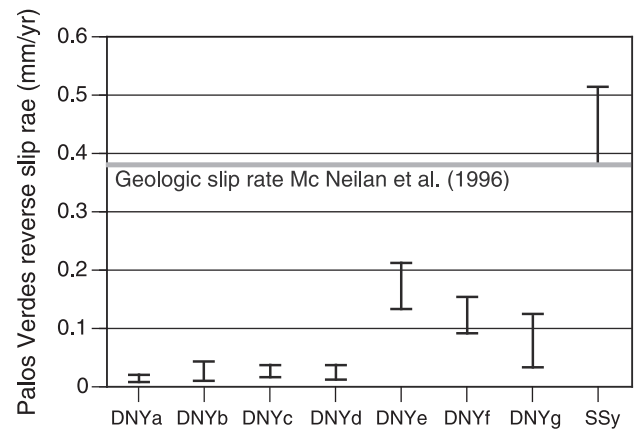


Figure 8. Reverse-slip rates along the Palos Verdes fault within the mechanical models. The range of slip is calculated from maximum and average slip along the modeled fault.

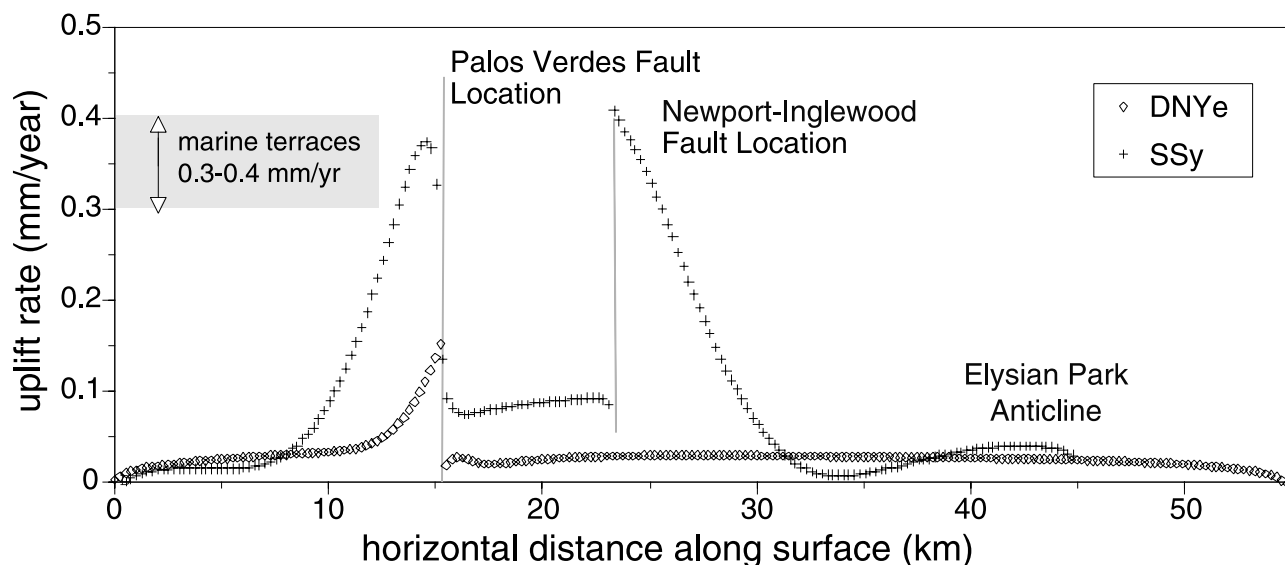


Figure 9. Surface uplift rates along the models. The two-dimensional nature of these models does not permit simulation of right-lateral slip; the uplift is a direct consequence of dip-slip along the faults. Uplift rate of the Palos Verdes Hills associated with dip slip on the Palos Verdes fault matches estimates from marine terrace data [McNeilan *et al.*, 1996] for SSy. However, the modeled uplift due to dip slip along the Newport-Inglewood fault exceeds our expectation. Although local uplift is observed along the Newport-Inglewood trend [Wright, 1991], this uplift is believed to result from folding associated with right-lateral slip along echelon fault segments rather than dip slip on the fault [Harding, 1973]. Reliable comparison of uplift of the Elysian Park anticline with paleoseismic observations [Oskin *et al.*, 2000] is not possible due to the boundary effects of the SSy model.

maximum) is the closest to the geologically determined reverse slip rate (0.38 mm yr^{-1} [McNeilan *et al.*, 1996]). The Palos Verdes fault dip-slip rates within the DNY models are at least 0.2 mm yr^{-1} less than the geologically determined rates. Whereas Palos Verdes fault slip rates inferred from kinematic analyses greatly exceed those determined from shallow geophysical evidence (Figure 3), the mechanical rates are within 1 order of magnitude of the geologic rates for most cross sections and surprisingly close for the Shaw and Suppe [1996] cross section. Potential sources of the discrepancy between kinematic and mechanically derived slip rates are discussed later in this paper.

[32] In addition to slip rates on the Palos Verdes fault we can compare uplift rates of the Palos Verdes Hills derived from the ages of exhumed marine terraces. Uplift rates generally range from 0.3 to 0.4 mm yr^{-1} [McNeilan *et al.*, 1996]. Within our mechanical models, uplift of the Palos Verdes Hills varies with location along the cross section and fault configuration (Figure 9). The SSy model has maximum uplift rates nearest the range of the geologic uplift rates. In summary, the mechanical simulation based on Shaw and Suppe's [1996] cross section has a surprisingly close match to the paleoseismic uplift and dip-slip rates of the Palos Verdes Hills and fault. The results for Palos Verdes suggest (1) that of the proposed configurations, SSy provides the closest match and (2) that the mechanical simulations of slip more closely match observations than the kinematic estimates.

4.3.2. Newport-Inglewood fault

[33] Although the direct evidence for dip slip along the Newport-Inglewood fault is inconclusive, indirect evidence suggests limited Quaternary dip slip along this fault. Stratigraphic evidence [Harding, 1973; Wright, 1991] and seis-

micity [Hauksson, 1987] suggest that we should expect little dip slip on the Newport-Inglewood fault within the mechanical models; however, one of the models of this study produces significant reverse slip on this fault.

[34] The SSy model produces dip slip on the Newport-Inglewood fault of 0.06 – 0.37 mm yr^{-1} , (average maximum slip rate). In contrast, the Newport-Inglewood fault within all other models, DNYa–DNYg, does not slip within the simulated 55,500 years of contraction. The excessive reverse slip along this fault in SSy is a consequence of fault interaction rather than favorable orientation of this fault segment. At shallow levels the Newport-Inglewood fault dips steeply and is not favorably oriented for slip under horizontal contraction (Figures 2 and 5). Although the Newport-Inglewood fault within the DNY models is isolated and does not slip, the fault in SSy is connected to a more gently dipping bed-parallel detachment to the east. Abundant reverse slip along this shallow and more favorably oriented fault promotes slip along the steep segment of the Newport-Inglewood fault (Figures 5 and 9). Thus the interaction of faults in SSy produces a slip pattern not expected by analysis of individual faults. To correct the excessive reverse dip slip on the Newport-Inglewood fault, we modify the fault configuration of the SSy model.

5. Modified Cross Section

[35] Multiple viable fault systems can match the surface and seismic expressions of folding in the Los Angeles Basin. Although the interpretation of Shaw and Suppe [1996, Figure 1b] (Figure 2) produces excessive dip slip on the Newport-Inglewood fault in our mechanical models, another

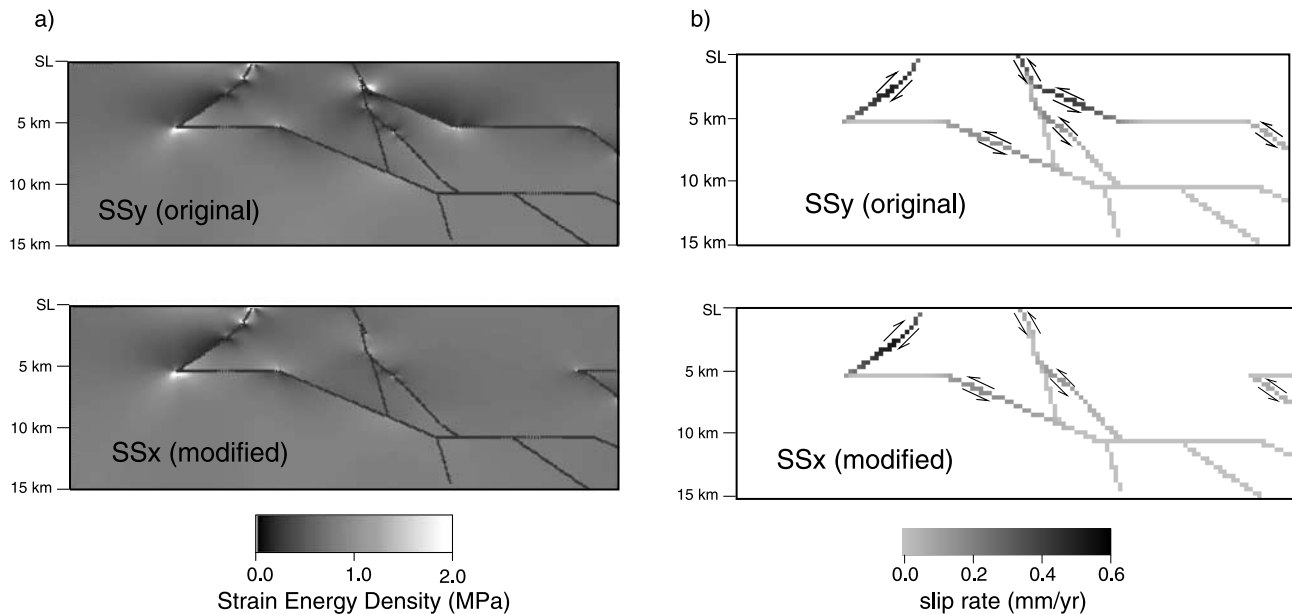


Figure 10. Comparison of (a) strain energy density and (b) slip distribution for SSy (original) and SSx (modified) fault models based on *Shaw and Suppe* [1996]. The modified model has fewer Navier-Coulomb stress concentrations due to removal of the shallow detachment fault. Additionally, the dip slip along the shallow segment Newport-Inglewood fault is reduced.

fault configuration might match the surface and seismic evidence of folding as well as the paleoseismic dip-slip rates. To test this, we modify the fault system of SSy by removing the shallow detachment under the central plain of the Los Angeles Basin and incorporating a wedge fault geometry for the Puente Hills thrust fault. Rather than transferring slip to the shallow detachment [*Shaw and Shearer*, 1999], the Puente Hills thrust ramp in the modified section forms a wedge with a suprajacent bedding-parallel detachment surface acting as a backthrust (Figure 10). This wedge fault system resembles that interpreted by *Shaw and Suppe* [1996] for cross section X-X' through the Coyote Hills, south of the transect investigated in this study [*Shaw and Suppe*, 1996, Figure 1a]. With excellent subsurface imaging, wedge and

ramp-detachment fault configurations could be distinguished based on active growth of either the synclinal or anticlinal axial surfaces; however, inconclusive imaging allows both fault configurations to be kinematically viable in the Puente Hills region (J. H. Shaw, personal communication, 2001). The modified wedge fault configuration produces a suprajacent west dipping monocline similar to that produced by the ramp-detachment configuration. In the following discussion the modified model is referred to as SSx.

[36] The modified cross section has similar slip rates and uplift rates of the Palos Verdes fault and hills as SSy (Figures 10 and 11). The modeled reverse dip-slip rate on the Palos Verdes fault in SSx, 0.40–0.54 mm yr⁻¹ (average to maximum), is only slightly greater than that for SSy and a close

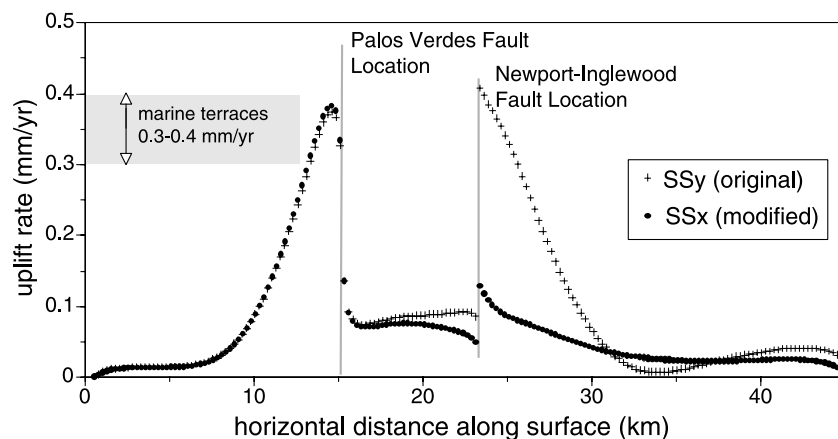


Figure 11. Surface uplift along the original SSy (original) and SSx (modified) models. The SSx uplift rate of the Palos Verdes Hills is close to both original SSy rate and the rate determined from marine terrace ages. The reduction in reverse slip along the Newport-Inglewood fault due to modification of the model produces a corresponding reduction of surface uplift associated with this fault.

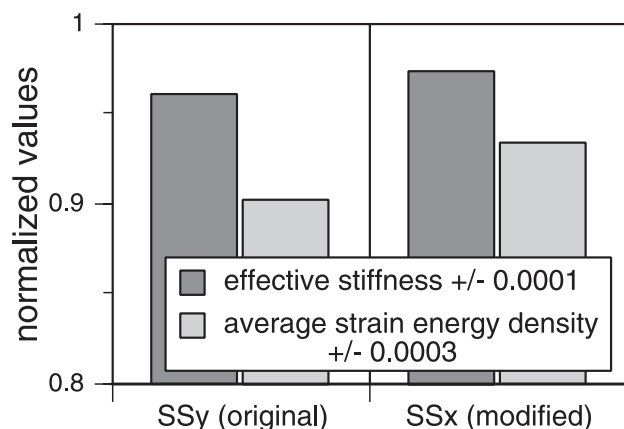


Figure 12. Normalized effective stiffness and average strain energy density for SSy and SSx (modified) models. The modified model has greater stiffness and greater average strain energy density than the SSy model with the shallow detachment. The modification reduces the overall mechanical efficiency.

match to the geologically determined rate. The removal of the shallow detachment reduces the slip potential on the Newport-Inglewood fault thereby reducing the near-surface reverse slip on this fault to 0.10 mm yr^{-1} ($\sim 25\%$ of the SSy dip slip rate Figure 10). The SSx dip-slip rate better fits our expectations for the Newport-Inglewood fault than the SSy model. Interestingly, the bed-parallel back thrust of the Puente Hills Thrust in SSx does not slip (Figure 10). Thus the slip distribution along the Puente Hills thrust in this mechanical model forms a blind thrust fault that terminates into a fault-tip fold.

[37] The SSx model has greater effective stiffness and greater average strain energy density than the SSy model. With the modification the average strain energy density normalized by the faultless model increases from 0.9006 ± 0.0003 to 0.9330 ± 0.0003 and the normalized effective stiffness increases to 0.9728 ± 0.0001 (Figure 12). Thus, SSx represents a mechanically less-efficient fault system than SSy, as there is less fault slip and greater storage of strain within the host rock. However, the average strain energy density of the modified SSx model is much less than the DNY a–g models, indicating relatively greater mechanical efficiency of this fault system. In summary, the SSx model has the closest match to the paleoseismic evidence yet has slightly lower mechanical efficiency than SSy model.

6. Discussion

[38] The mechanical modeling of this study serves two purposes. The first is to evaluate among proposed two-dimensional cross-sections of faulting in the Los Angeles Basin and the second is to explore the use of mechanical efficiency as a new tool for evaluation among multiple viable fault models. To this end, we discuss the implications of the slip rates resulting from the mechanical models and the insights provided by the mechanical efficiency analysis.

6.1. Predicted Slip Rates

[39] The Palos Verdes slip rates produced by the mechanical models are less than the kinematically determined slip

rates. Within the kinematic analysis, reverse slip along the Palos Verdes fault is not directly assessed from associated fold shape; rather, slip along Palos Verdes is inferred from slip along the nearby Compton ramp, for which overlying folding provides slip evidence [Shaw and Suppe, 1996]. The horizontal contraction along the Compton ramp is balanced with equal horizontal contraction along the Palos Verdes fault. Consequently, the kinematic assumption that slip along the Compton ramp directly relates to slip along the Palos Verdes fault contributes to the discrepancy between kinematic and mechanical slip estimates. Within the mechanical model dip slip along the Palos Verdes fault is not directly related to slip along the Compton ramp because the host rock locally deforms (dilates or contracts, e.g., Figure 6) producing nonuniform slip along the faults (Figure 5). Because the mechanical dip-slip rate on the Compton ramp ($0.09\text{--}0.15 \text{ mm yr}^{-1}$) is much less than the kinematic estimate ($1.4 \pm 0.4 \text{ mm yr}^{-1}$ [Shaw and Suppe, 1996]) other factors must also contribute to the discrepancy between the estimates.

[40] Another contributor to the discrepancy between slip rates may be the difference in time spans used to estimate slip. Slip along the Compton ramp is calculated from folding of 2–2.5 Myr strata overlying the ramp. A difference between recent strain rates measured via geodesy and Pliocene deformation rates could account for some discrepancy in estimated slip rates. The uniform uplift of the Palos Verdes peninsula over the last 1 Myr [Ward and Valensise, 1994] suggests uniform contraction over this time span however we have no evidence for constant contraction rates in the Los Angeles Basin over the last 2.5 Myr.

[41] The fault slip rates for the Palos Verdes and Newport-Inglewood faults predicted by the mechanical models more closely match the paleoseismic slip rates than the kinematic models. This result suggests that the mechanical models with geodetic strain as boundary conditions may better estimate recent fault slip rates than kinematic models that average slip over much longer time spans. Correlations of seismic hazard with maximum slip rate along faults [e.g., Dolan et al., 1995; Petersen et al., 1996; Oskin et al., 2000] suggest that the mechanical models may estimate lower levels of seismic hazard along the blind thrust faults within the studied transect than the kinematic models.

[42] Because the deep subsurface geometry of the Palos Verdes fault system is ill-constrained, alternative configurations may yield similar overlying fold shapes yet different slip rates within the mechanical models. Kinematic methodologies can be used to provide alternative fault configurations [e.g., Shaw and Suppe, 1996] as well as estimates of the overall slip rates on geologic timescales. Thus we recommend an integrated approach in seismic hazard assessment utilizing both kinematic tools to develop multiple viable fault models from structural data and mechanical models to evaluate the viability of these models. The mechanical models can be used to match the geologically determined slip rates and mechanical efficiency can be used to evaluate among the models.

[43] Some faults within the mechanical models do not slip under the simulated 55,500 years of contraction. Horizontal detachments are unfavorably oriented for slip under horizontal contraction. Increasing the dip of detachments could yield increased slip along these fault segments. We

expect that such modifications would provide increased fault slip along deeper faults and subsequently increase the overall mechanical efficiency of the models.

[44] Within the models, faults below about 10 km depth also do not slip. One contributor to the lack of slip at depth is increased compression, which inhibits fault slip; however host rock and fault rheology also influence fault slip. The models within this study consist of homogeneous and linear elastic host rock; however, the heterogeneous architecture of crystalline basement overlain by sedimentary strata within the Los Angeles Basin may influence the distribution of slip along faults. The highly stiff crystalline rock may resist elastic deformation and consequently promote fault slip within the basement. Additionally, at depths below ~15 km the deformation of faults may be more accurately simulated with a viscous-elastic rheology rather than the coulomb friction criterion used in this study. Within 55,500 years of horizontal contraction, a viscous-elastic fault zone may experience much greater slip than a fault that only slips under the static coulomb friction criterion.

6.2. Local Versus Global Mechanical Efficiency

[45] This study illuminates the competing factors of mechanically efficient interactions between individual faults and mechanical efficiency of the entire fault system. Two slipping faults that interfere with one another can produce local SED concentrations, which inefficiently strain the host rock. However, the average SED results show that locally inefficient fault interactions, such as within SSy, do not necessarily decrease the global mechanical efficiency; some fault networks without SED concentrations (e.g DNYe) are less efficient than SSy. The difference in fault network efficiency may be a consequence of differing amounts of overall slip along all faults within the system; SSy has much greater levels of fault slip than DNYe and consequently has greater strain shadows adjacent to slipping faults. This relationship is further supported by the reduction in mechanical efficiency that accompanied the removal of several slipping fault segments from the original SSy system. The results of this study suggest that greater fault slip yields greater overall mechanical efficiency of fault networks even if some faults interfere with one another.

[46] In the future, these mechanical efficiency parameters may be used to investigate the increase in mechanical efficiency during fault system evolution and the nature of three-dimensional deformation within the Los Angeles Basin. Three-dimensional interactions between reverse, oblique, and strike-slip faults are far more complex than the two-dimensional interactions investigated within this study. Consequently, quantification of fault network mechanical efficiency may be quite valuable for assessing three-dimensional fault configuration. This two-dimensional study lays the groundwork for further three-dimensional mechanical analysis of the Los Angeles Basin.

[47] The measures of mechanical efficiency presented in this study (effective stiffness and strain energy density) provide convenient quantification of fault system behavior. The effective stiffness and average strain energy density express the cumulative influence of individual fault interactions on the overall mechanical efficiency of a fault system. Hence locally inefficient fault interactions may or may not significantly impact the efficiency of the entire

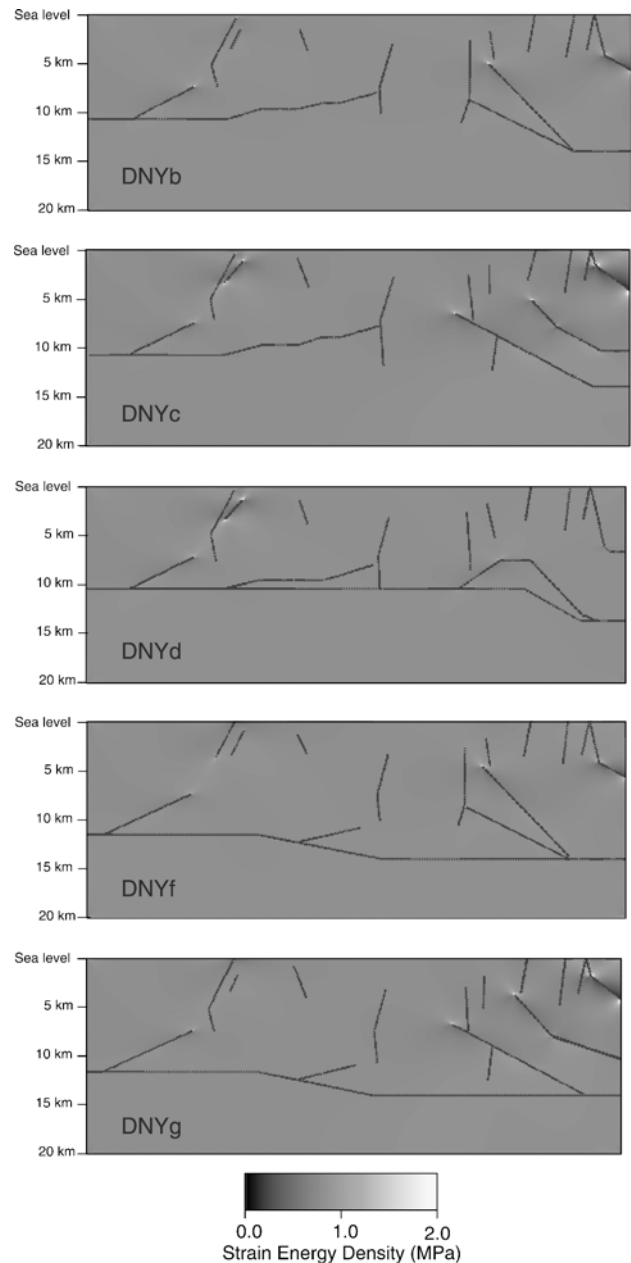


Figure A1. Strain energy density of models DNYb, DNYc, DNYd, DNYf, and DNYg. Brighter areas indicate greater values of strain energy density.

system. Mechanical efficiency may be a powerful tool for the investigation of fault interaction within complex fault systems because it evaluates the cumulative effect of frictional fault interaction on the entire system rather than individual faults.

7. Conclusions

[48] The eight proposed cross sections of *Davis et al.* [1989] and *Shaw and Suppe* [1996] all match the surface and, to some degree, the seismic expression of subsurface structures. Testing of the proposed fault configurations with mechanical boundary element method models shows that the slip rates and uplift rates of the Palos Verdes fault and

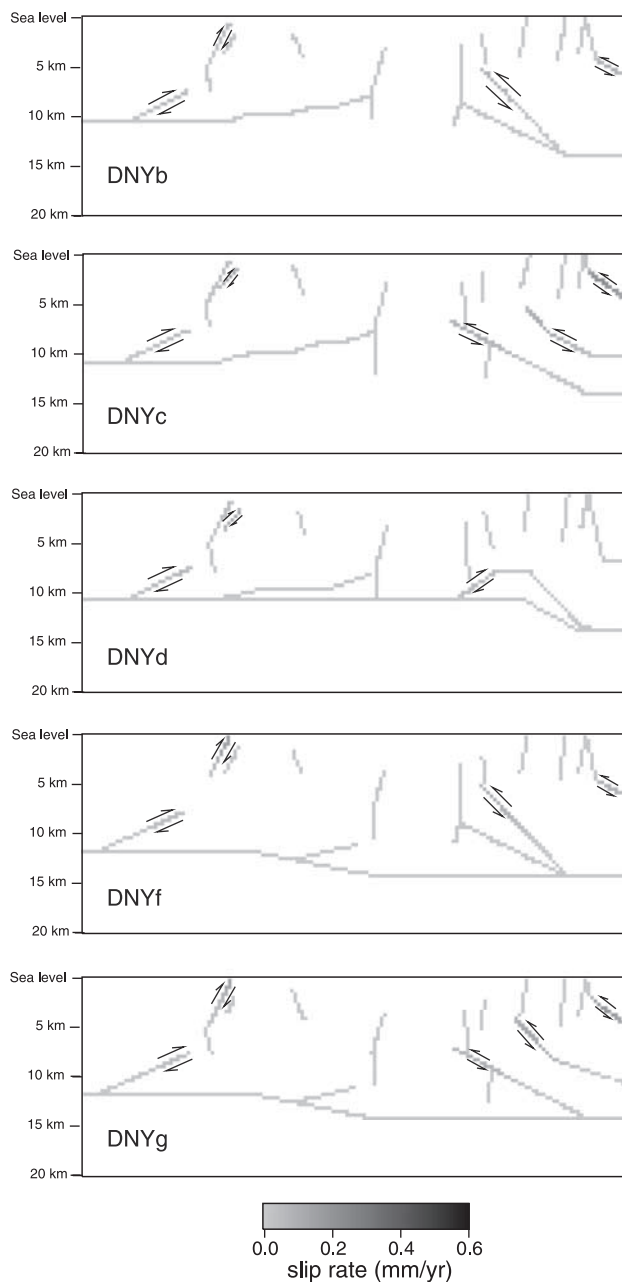


Figure A2. Slip distribution of models DNYb, DNYc, DNYd, DNYf, and DNYg. Arrows indicate sense of slip.

hills for the *Shaw and Suppe* [1996] fault system best match the geologically determined values. This cross section also has the greatest mechanical efficiency owing to the high degree of fault connectedness in the section.

[49] Large dip-slip rates produced on the Newport-Inglewood in the mechanical model based on *Shaw and Suppe* [1996] lead us to suspect that the fault network in their proposed cross section is overly connected. A modification to the *Shaw and Suppe* [1996] cross section produces lesser mechanical efficiency than the original section but better correlation with geologic observations. This modification eliminates the shallow (~ 5 km) detachment proposed just west of the Newport-Inglewood fault so that the monocline of the Whittier Hills is produced by an underlying fault propagation or wedge fault geometry. This study shows that

the most appropriate fault configuration for a region may not necessarily be that with the greatest overall mechanical efficiency; rather, the most viable fault system should match the available geologic observations. Furthermore, slip rates from the mechanical models are less than the kinematically derived rates and closer to available geologically determined rates. The mechanical models may more accurately simulate the deformation throughout an interacting fault network because they include host rock deformation and of more recent strain rates.

[50] Studying isolated faults provides limited knowledge of earthquake source parameters because fault systems are composed of interacting faults that alter each other's earthquake potential [e.g., *Harris*, 1998]. We believe that studies of fault interaction can enhance earthquake hazard assessment by improving source characteristics used for constraining maximum probable/possible earthquakes. In a location such as in the Los Angeles Basin where many faults are buried and therefore inaccessible for direct observation, improvement of techniques to infer slip rates from indirect evidence becomes crucial. Effective stiffness and strain energy density are valuable quantitative parameters for furthering our understanding of fault interactions and, in conjunction with geodetic information on active strain rates and rheological fault models, offer great potential for future applications. The mechanical assessment of the Los Angeles Basin illuminates the importance of understanding complex fault interaction, in particular, how local faults interact within a single regional fault system.

Appendix A

[51] Two representative cross sections by *Davis et al.* [1989] were presented, DNYa and DNYe. The slip distribution (Figure A1) and strain energy density (Figure A2) for the remaining five sections are presented here.

[52] **Acknowledgments.** The paper greatly benefited from reviews by James Dolan, Ruth Harris, and Jan Vermilye as well as discussions with Susan Murphy. This study was supported by NEHRP grant 98-HQ-GR-1025 to Michele L. Cooke and a UW-Madison Geology and Geophysics Weeks Graduate Fellowship to Ayako Kameda.

References

- An, L.-J., and C. G. Sammis, A cellular automation for the development of crustal shear zones, *Tectonophysics*, 253, 247–270, 1996.
- Bandy, O. L., and L. Marincovich Jr., Rates of Late Cenozoic uplift, Baldwin Hills, Los Angeles, California, *Science*, 181, 653–655, 1973.
- Birch, F., Compressibility; elastic constants, in *Handbook of Physical Constants*, edited by J. S. P. Clark, pp. 97–173, Geol. Soc. of Am., Boulder, Colo., 1966.
- Bird, P., and X. Kong, Computer simulations of California tectonics confirm very low strength of major faults, *Geol. Soc. Am. Bull.*, 106, 159–174, 1994.
- Bryant, M. E., Emergent marine terraces and Quaternary tectonics, Palos Verdes Peninsula, California, in *Geology of the Palos Verdes Peninsula and San Pedro Bay, SEPM Guidebook*, edited by P. J. Fischer et al., pp. 63–78, Soc. of Econ. Paleontol. and Mineral., Tulsa, Okla., 1987.
- Carmichael, R. S., *CRC Handbook of Physical Properties of Rocks*, CRC Press, Boca Raton, Fla., 1984.
- Castle, R. O., and J. M. Buchanan-Banks, Vertical surface displacements along a part of the Newport-Inglewood zone of folds and faults, Los Angeles and Orange Counties, California, U.S. Geol. Surv., Reston, Va., 1989.
- Clark, M. M., et al., Preliminary slip-rate table and map of late-Quaternary faults of California, *U.S. Geol. Surv. Open File Rep.*, 84-0106, 1984.

- Cooke, M., and C. Underwood, Fracture termination and step-over at bedding interfaces due to frictional slip and interface debonding, *J. Struct. Geol.*, **23**, 223–238, 2001.
- Cooke, M., P. Mollema, D. Pollard, and A. Aydin, Interlayer slip and joint localization in East Kaibab Monocline, Utah: Field evidence and results from numerical modeling, in *Forced Folds and Fractures*, edited by J. W. Cosgrove, and M. S. Ameen, *Geol. Soc. Spec. Publ.*, **169**, 23–49, 2000.
- Cooke, M. L., and D. D. Pollard, Bedding-plane slip in initial stages of fault-related folding, *J. Struct. Geol.*, **19**, 567–581, 1997.
- Cowie, P. A., D. Sornette, and C. Vanneste, Multifractal scaling properties of a growing fault population, *Geophys. J. Int.*, **122**, 457–469, 1995.
- Crouch, S. L., Computer simulation of mining in faulted ground, *J. S. Afr. Inst. Min. Metall.*, **79**, 159–173, 1979.
- Crouch, S. L., and A. M. Starfield, *Boundary Element Methods in Solid Mechanics*, Chapman and Hall, New York, 1990.
- Dahlen, F. A., and T. D. Barr, Brittle frictional mountain building, 1, Deformation and mechanical energy budget, *J. Geophys. Res.*, **94**, 3906–3922, 1989.
- Davis, T. L., J. Namson, and R. F. Yerkes, A cross section of the Los Angeles area: Seismically active fold and thrust belt, the 1987 Whittier Narrows earthquake, and earthquake hazard, *J. Geophys. Res.*, **94**, 9644–9664, 1989.
- Deng, J., and L. R. Sykes, Evolution of the stress field in southern California and triggering of moderate-sized earthquakes: A 200-year perspective, *J. Geophys. Res.*, **102**, 9859–9886, 1997.
- Dolan, J. F., K. Sieh, T. K. Rockwell, R. S. Yeats, J. Shaw, J. Suppe, G. J. Huftile, and E. M. Gath, Prospects for larger or more frequent earthquakes in the Los Angeles metropolitan region, *Science*, **267**, 199–205, 1995.
- Dolan, J. F., D. Stevens, and T. K. Rockwell, Paleoseismologic evidence for an early to mid-Holocene age of the most recent surface rupture on the Hollywood Fault, Los Angeles, California, *Bull. Seismol. Soc. Am.*, **90**, 334–344, 2000.
- Duebendorfer, E. M., J. Vermilye, P. A. Geiser, and T. L. Davis, Evidence for aseismic deformation in the western Transverse Ranges, southern California: Implications for seismic risk assessment, *Geology*, **26**, 271–274, 1998.
- Feigl, K. L., et al., Space geodetic measurement of crustal deformation in central and southern California, 1984–1992, *J. Geophys. Res.*, **98**, 21,677–21,712, 1993.
- Fischer, P. J., J. H. Rudat, R. H. Patterson, and G. Simila, The Palos Verdes fault zone: Onshore to offshore, in *Geology of the Palos Verdes Peninsula and San Pedro Bay*, edited by P. J. A. M. I. Fischer, pp. 91–133, Am. Assoc. of Pet. Geol., Tulsa, Okla., 1987.
- Freeman, S. T., E. G. Heath, P. D. Guptill, and J. T. Waggoner, Seismic hazard assessment, Newport-Inglewood Fault, in *Engineering Geology Practice in Southern California*, edited by B. W. Popkin and R. J. Proctor, Assoc. of Eng. Geol., Belmont, Calif., 1992.
- Grant, L. B., J. T. Waggoner, T. K. Rockwell, and C. von Stein, Paleoseismicity of the north branch of the Newport-Inglewood fault zone in Huntington Beach, California, from cone penetrometer test data, *Bull. Seismol. Soc. Am.*, **87**, 277–293, 1997.
- Gupta, S., P. A. Cowie, N. H. Dawers, and J. R. Underhill, A mechanism to explain rift-basin subsidence and stratigraphic patterns through fault array evolution, *Geology*, **26**, 595–598, 1998.
- Hardebeck, J., J. Nazareth, and E. Hauksson, The static stress change triggering model: Constraints from two southern California aftershock sequences, *J. Geophys. Res.*, **103**, 24,427–24,437, 1998.
- Harding, T. P., Newport-Inglewood trend, California: An example of wrenching style of deformation, *Am. Assoc. Pet. Geol. Bull.*, **57**, 97–116, 1973.
- Harris, R. A., Stress triggers, stress shadows, and implications for seismic hazard: Introduction to the special issue, *J. Geophys. Res.*, **103**, 24,347–24,358, 1998.
- Hauksson, E., Seismotectonics of the Newport -Inglewood fault zone in the Los Angeles Basin, southern California, *Bull. Seismol. Soc. Am.*, **77**, 539–561, 1987.
- Hauksson, E., and L. M. Jones, The 1987 Whittier Narrows earthquake sequence in Los Angeles, southern California: Seismological and tectonic analysis, *J. Geophys. Res.*, **94**, 9569–9589, 1989.
- Ingersoll, R. V., and P. E. Rumelhart, Three-stage evolution of the Los Angeles Basin, southern California, *Geology*, **27**, 593–596, 1999.
- Jones, L. M., et al., The magnitude 6.7 Northridge, California, earthquake of 17 January 1994, *Science*, **266**, 389–397, 1994.
- Kagan, Y. Y., Are earthquakes predictable?, *J. Geophys. Int.*, **131**, 505–525, 1997.
- King, G. C. P., R. S. Stein, and J. Lin, Static stress changes and the triggering of earthquakes, *Bull. Seismol. Soc. Am.*, **84**, 935–953, 1994.
- McNeilan, T. W., T. K. Rockwell, and G. S. Resnik, Style and rate of Holocene slip, Palos Verdes Fault, southern California, *J. Geophys. Res.*, **101**, 8317–8334, 1996.
- Mitra, G., and S. E. Boyer, Energy balance and deformation mechanisms of duplexes, *J. Struct. Geol.*, **8**, 291–304, 1986.
- Nicholson, C., C. C. Sorlien, T. Atwater, J. C. Crowell, and B. P. Luyendyk, Microplate capture, rotation of the western Transverse Ranges, and initiation of the San Andreas transform as a low-angle fault system, *Geology*, **22**, 491–495, 1994.
- Norris, R. M., and R. W. Webb, *Geology of California*, John Wiley, New York, 1990.
- Oskin, M., K. Sieh, T. Rockwell, G. Miller, P. Guptill, M. Curtis, S. McArdle, and P. Elliot, Active parasitic folds on the Elysian Park Anticline: Implications for seismic hazard in central Los Angeles, California, *Geol. Soc. Am. Bull.*, **112**, 693–707, 2000.
- Petersen, M. D., and S. G. Wesnousky, Fault slip rates and earthquake histories for active faults in southern California, *Bull. Seismol. Soc. Am.*, **4**, 1608–1649, 1994.
- Petersen, M. D., C. H. Cramer, W. A. Bryant, M. S. Reichle, and T. R. Toppozada, Preliminary seismic hazard assessment for the Los Angeles, Ventura, and Orange Counties, California, affected by the 1 January 1994 Northridge earthquake, *Bull. Seismol. Soc. Am.*, **86**, S247–S261, 1996.
- Reiter, M., *The Palos Verdes Peninsula: A Geologic Guide and More*, Kendall Hunt, Dubuque, Iowa, 1984.
- Roering, J. J., M. L. Cooke, and D. D. Pollard, Why blind thrust faults do not propagate to the Earth's surface: Numerical modeling of coseismic deformation associated with thrust-related anticlines, *J. Geophys. Res.*, **102**, 11,901–11,912, 1997.
- Schenk, V., Achievements and probable trends in seismic hazard assessment, *Tectonophysics*, **167**, 157–169, 1989.
- Scholz, C. H., *The Mechanics of Earthquakes and Faulting*, Cambridge Univ. Press, New York, 1990.
- Scholz, C. H., Evidence for a strong San Andreas Fault, *Geology*, **28**, 163–166, 2000.
- Shaw, J. H., and P. M. Shearer, An elusive blind-thrust fault beneath metropolitan Los Angeles, *Science*, **283**, 1516–1518, 1999.
- Shaw, J. H., and J. Suppe, Earthquake hazards of active blind-thrust faults under the central Los Angeles Basin, California, *J. Geophys. Res.*, **101**, 8623–8642, 1996.
- Shen, Z.-K., D. D. Jackson, and B. X. Ge, Crustal deformation across and beyond the Los Angeles Basin from geodetic measurements, *J. Geophys. Res.*, **101**, 27,957–27,980, 1996.
- Stephenson, W. J., T. K. Rockwell, J. I. Odum, K. M. Shedlock, and D. A. Okaya, Seismic reflection and geomorphic characterization of the onshore Palos Verdes fault zone, Los Angeles, California, *Bull. Seismol. Soc. Am.*, **85**, 943–950, 1995.
- Suppe, J., R. E. Bischke, and J. Shaw, Regional map view and cross-sectional determination of fault geometry and slip for blind thrusts in populated areas of southern California, paper presented at SCEC Annual Meeting, S. Calif. Earthquake Cent., Los Angeles, Calif., 1992.
- Timoshenko, S. P., and J. N. Goodier, *Theory of Elasticity*, McGraw-Hill, New York, 1934.
- Vermilye, J. M., and L. Seeber, Pressure solution strain analysis for the San Cayetano Fault: Aseismic deformation associated with a seismogenic fault, *Geol. Soc. Am. Abstr. Programs*, **30**, 325, 1998.
- Walls, C., T. Rockwell, K. Mueller, Y. Block, S. Williams, J. Pfanner, J. Dolan, and P. Fang, Escape tectonics in the Los Angeles metropolitan region and implications for seismic risk, *Nature*, **394**, 356–360, 1998.
- Ward, S. N., and G. Valensise, The Palos Verdes terraces, California: Bath-tub rings from a buried reverse fault, *J. Geophys. Res.*, **99**, 4485–4494, 1994.
- Wesnousky, S. G., Seismological and structural evolution of strike-slip faults, *Nature*, **335**, 340–343, 1988.
- Wright, T. L., Structural geology and tectonic evolution of the Los Angeles Basin, California, *AAPG Mem.*, **52**, 35–134, 1991.
- Yeats, R. S., Newport-Inglewood fault zone, Los Angeles Basin, California, *Am. Assoc. Pet. Geol. Bull.*, **57**, 117–135, 1973.
- Yeats, R. S., and J. M. Beall, Stratigraphic controls of oil fields in the Los Angeles Basin: A guide to migration history, in *Active Margin Basins*, edited by K. T. Biddle, *AAPG Mem.*, **52**, 221–235, 1991.
- Yerkes, R. F., *Geology of the Los Angeles Basin, California: An introduction*, *U.S. Geol. Surv. Prof. Pap.*, **0420-A**, A1–A57, 1965.

M. L. Cooke, Geosciences Department, University of Massachusetts-Amherst, 611 North Pleasant Street, Amherst, MA 01003, USA. (cooke@geo.umass.edu)

A. Kameda, Geological and Environmental Sciences Department, Stanford University, 450 Serra Mal Bldg 320, Stanford, CA 94305-2115, USA.